The influence of shear on the metabolite yield of *Lactobacillus rhamnosus* biofilms

Hendrik Gideon Brink[a], Willie Nicol[a](Corresponding Author)

[a]*University of Pretoria, Department of Chemical Engineering, University of Pretoria, Lynnwood Road, Hatfield, Pretoria, 0002, South Africa*

Corresponding Author:

Willie Nicol

Tel: +2712 420 3796

Fax: +2712 420 5048

Email: willie.nicol@up.ac.za

Postal Address: Willie Nicol

University of Pretoria

Department Chemical Engineering

Pretoria

South Africa

0002

Abstract

A tubular recycle bioreactor was employed to ensure homogeneous shear conditions on the biofilm surface. Superficial liquid velocities of 0.19 $m.s^{-1}$, 0.37 $m.s^{-1}$, 0.55 $m.s^{-1}$ and 3.65 $m.s^{-1}$ were used. The highest velocity resulted in negligible cell attachment (chemostat) while the ratio of attached-to-total cell mass escalated as the superficial velocity decreased. The lactic acid yield on glucose increased from 0.75 $g.g^{-1}$ to 0.90 $g.g^{-1}$ with declining shear while the corresponding acetoin yield on glucose decreased from 0.074 $g.g^{-1}$ to 0.017 $g.g^{-1}$. Redox analysis of the catabolites revealed a net consumption of NADH in the anabolism, while the extent of NADH consumption decreased when shear was reduced. This was attributed to the formation of more extracellular polymeric substances (EPS) at low shear conditions. A simplified metabolic flux model was used to estimate the EPS content of the biomass as a function of the shear velocity. Rate data supported the notion of increased EPS at lower shear.

Keywords: *Lactobacillus rhamnosus*, Biofilms, Extracellular Polymeric Substance, Metabolic Flux Distribution, Lactic Acid, Acetoin.

INTRODUCTION

It is well established that some microbial strains have the potential to self-adhere to support surfaces. From a bioprocessing perspective, this property can be utilized to increase the biomass content in a bioreactor and, correspondingly, the volumetric productivity. Self-immobilisation is one of the simplest forms of cell retention in a bioreactor where no active separation is required [1,2]. Biofilms are utilised in various biological industries such as waste degradation and nutrient consumption [1,3–6], natural ecosystems [7] and some conventional fermentation processes [4,6]. From an academic perspective, biofilm reactors are much less favoured than their suspended cell counterparts, since biomass quantification for biofilm reactors is more difficult and more intrusive than for suspended cell reactors where an outlet sample reflects the same biomass concentration as the reactor [2,8–11]. Biofilm reactors require extensive periods to develop mature biofilms and continuous or repeat batch setups are typically employed to achieve this. Due to the prolonged operating times of these reactor types, the sterility challenges are more severe while steady-state takes longer to achieve. All this contributes to biofilm reactors being unfavourable for fundamental investigations.

From an industrial perspective, the self-immobilisation property of biofilm reactors remains attractive, especially with regard to equipment cost where expensive separation schemes can be avoided. With the dawning age of the biorefinery, fermentation is seen in a new light and microorganism catabolites are likely to form an integral part of the commodity chemicals of tomorrow. This places greater focus on bioreactor efficiency where improved design can have a major impact on the process economics. It is projected that numerous fermentation-based chemicals will be produced on a bulk scale, similar to that of conventional petrochemical-based chemicals [12,13]. In this respect, the fundamental advantages of high cell density continuous production [14] become more significant and tie in with biofilm reactors in which prolonged fermentation times are required. From a bioprocessing point of view, the production characteristics of biofilms are relatively unexplored, with most work concentrating on the productivity enhancement caused by the biomass increase [1,2,6,15] and the robustness and stability of prolonged continuous

operation [6]. Metabolite yield differences have been reported when comparing biofilm reactors to their suspended cell counterparts [16–18] although no attempt was made to elucidate the cause of the differences.

Metabolic flux analysis has become a powerful tool for understanding and manipulating metabolite distributions [19,20] in order to enhance the yield of the targeted molecule. The combined metabolic network demonstrates how the various parts influence each other due to common factors, such as adenosine triphosphate (ATP) and nicotinamide adenine dinucleotide (NAD^+/NADH), which are exchanged throughout the network. Given known metabolic pathways, redox closures and energy (ATP) balances can be used to calculate the flux of the excreted products. From a carbon flux perspective, microbial biofilms are unique in the sense that a fraction of the carbon source ends up as extracellular polymeric substances (EPS) [21]. Despite constituting a small loss of carbon (unless EPS are the desired product [22]), this additional carbon flux has the potential to influence the distribution of the metabolic network where the yield of the targeted metabolite can be affected. Depending on the redox and energy implications of the flux shift the yield change can be advantageous to the fermentation process.

The present study addresses the effect of liquid shear rate on biofilm productivity and more importantly, the product distribution. The expectation is that shear will affect the distribution of cells and EPS in the biofilm matrix [10]. Lactic acid (HLac) fermentation was chosen in order to minimize gas formation in the novel, shear-control fermenter used in the study. Numerous *Lactobacillus* species are known for their biofilm formation characteristics [1] and *Lactobacillus rhamnosus* ATCC 9595 was chosen for the fermentation. The biofilm properties of this organism are well studied [22–25] making it an ideal bacterium for the investigation. A tubular recycle fermenter was used that allows for a homogeneous distribution of the shear velocity over the external surface of the biofilm.

MATERIALS AND METHODS

Microorganism and growth medium

The microorganism used for the study was *L. rhamnosus* ATCC 9595. Stock cultures were stored at 6 °C on MRS agar slopes (Merck KgaA, Darmstadt, Germany). The growth medium for the seed culture was the same as that used for the reactor (described below) with 2 g $CaCO_3$ as a buffer agent, incubated for 18–24 hours at 37 °C.

Media

All chemicals were sourced from Merck KgaA (Darmstadt, Germany), unless specified differently. The medium used for the experimental runs consisted of ($g.L^{-1}$): glucose (Glc): 40; yeast extract (YE): 10; $MgSO_4.7H_2O$: 0.05; $MnSO_4.7H_2O$: 0.02; sodium acetate: 1.5; K_2HPO_4: 1; KH_2PO_4: 1; $FeSO_4.7H_2O$: 0.02; and ascorbic acid: 0.005. The Glc was diluted in 1.5 L of distilled water and the YE and mineral salts were diluted in 3.5 L of distilled water and separately sterilized by autoclaving at 121 °C for 40 min. Prior to use, the solutions were left to cool to room temperature, after which the glucose solution was aseptically added to the balance of the medium.

Bioreactor

The experimental setup used in the investigation is shown in Figure 1. It consists of a silicone tube of approximately 5 m length with an active volume of 46.1 mL (average inner diameter of 3.1 mm) in which the reaction takes place (shown in bold), a feed line, an NaOH dosing line, an inoculation line and a waste line. Nitrogen gas (Afrox, Johannesburg, South Africa) was connected to the feed sample line and the outlet line to prevent infection from the environment via the sampling point as well as maintaining anaerobic conditions.

Temperature was controlled at 37 °C using a hotplate coupled to a thermocouple, which was housed in an aluminium sheath connected within the reactor. pH was controlled at 6.25 by dosing unsterilized 4 M NaOH through a peristaltic pump 120U (Watson Marlow, Falmouth, UK) with a relay connected to a Liquiline CM442 controller and a Tophit CPS471D ISFET probe (Endress+Hauser, Gerlingen, Germany) housed within an inline stainless-steel holder. The CM442 was connected

to a data logging system NI USB-6008 (National Instruments, Austin, Texas) and pH, relay position and temperature were recorded continuously during fermentations.

The shear velocities (the quotient of the volumetric recycle rate ($m^3.s^{-1}$) and the cross sectional area (m^2) of the tube) used for the experiments were 3.65 m s^{-1} for the chemostat experiments and 0.55 $m.s^{-1}$, 0.37 $m.s^{-1}$ and 0.19 $m.s^{-1}$ for the biofilm experiments. Due to the high recycle rate, as compared with the reactor through flow, it was assumed that the reactor section acts as a perfectly mixed reactor with negligible axial and radial concentration profiles, typical ratios of recycle flow to the reactor through flow were between 175 and 17,700 [26]. This was confirmed by residence time distribution tests performed *in situ* by applying a pulse change to the NaOH for pH control and measuring the pH change over time. The production of HLac was continuously monitored by measuring the amount of NaOH dosed for pH control. This amount was assumed to be directly proportional to the production of HLac.

Product analysis

The bacterium possesses seven distinct metabolic products [27–29]: HLac, acetoin (Acn), diacetyl (Diac), pyruvic acid (HPyr), citric acid, oxaloacetic acid and acetic acid, the concentrations of which were measured, along with residual Glc using an Infinity 1260 high-performance liquid chromatograph (Agilent Technologies, USA) with an Aminex HPX-87H ion-exclusion organic acid column (Bio-Rad Laboratories, Berkeley, California). The column was pre-calibrated using > 99% purity standards sourced from Merck KgaA (Darmstadt, Germany) and (Sigma–Aldrich, St. Louis, Missouri). Only two products, HLac and Acn, were measured in appreciable quantities (> 0.1 $g.L^{-1}$). A simplified metabolic flux diagram (from [27–29]) for *L. rhamnosus* is shown in Figure 2 which shows that the carbon from Glc can be diverted towards the suspended biomass (x) and anabolic CO_2 (α) as well as catabolic products HLac and Acn and catabolically produced CO_2. The system was assumed to be fully anaerobic due to the absence of Diac in the product. Diac is produced by non-enzymatic oxidation of 2-acetolactate [30,31], the direct precursor to Acn, and therefore in the presence of oxygen one would expect the presence of Diac and *vice versa*.

Steady-state criteria

The steady-state in the system was predicted by an algorithm programmed in the data logging system, which integrated the accumulation rate of HLac over time ($C_{HLac}(t)$) (equation (1)) and compared that with the theoretical concentration of HLac at steady-state ($C_{HLac,steady}$) (equation (2)). The $C_{HLac,steady}$ (equation (3)) only has physical meaning at values where equations (1) and (2) have corresponding values. The value for $C_{HLac}(0)$ was determined at the initiation of each run by measuring the initial concentration of HLac in the reactor effluent.

$$C_{HLac}(t) = C_{HLac}(0) + \sum_{0}^{t_f} \left(q_{HLac}(t) - DC_{HLac}(t)\right) \Delta t \quad (1)$$

$$C_{HLac,steady} = \frac{q_{HLac}(t)}{D} \quad (2)$$

$$q_{HLac}(t) = \frac{(4)(90)Q_{NaOH}(t)}{V_R} \quad (3)$$

Figure 3 shows a typical profile of the calculated values of C_{HLac} and $C_{HLac,steady}$, from which it can be seen that despite the $C_{HLac}(t)$ fluctuating throughout the run, the $C_{HLac,steady}$ matches the $C_{HLac}(t)$. This indicates that a metabolic steady-state was reached despite fluctuations in the total biomass content (suspended and attached cells). As a precaution, the reactor effluent was analysed a period of 48 h after initiation for D > 0.2 h^{-1} and after 96 h for D < 0.2 h^{-1} since temporary pseudo steady states were observed in the initial stages of biofilm development. The longer times allowed at low dilution was due to slow growth at higher HLac titres. Samples were taken after the mentioned periods when the predicted $C_{HLac}(t)$ and $C_{HLac,steady}$ were equal.

Biomass quantification

Calibration curves of dry weight-to-absorbance were determined by measuring the absorbance of outlet samples from the reactor at different biomass outlet concentrations for wavelengths of 560 nm (T60 UV/VIS Spectrophotometer, PG Instruments, Leicestershire, UK). The samples were washed twice with distilled water, re-suspended in distilled water and dried overnight at 70 °C. The dry weights were calibrated to the measured absorbance of the samples. The biomass concentrations were inferred by comparing them with the pre-calibrated concentration-absorbance curves for the C_x (equations (4)) and sample biomass (C_S)

measured after the washout procedure described in the *Calculation of total biomass* section (equation (5)). Equations (4) and (5) fit the experimentally determined ABS_{560} to dry cell weight with r^2 values of 0.92 and 0.90 respectively, in the ABS_{560} range between 1.90 and 2.65.

$$C_x = 3.82(ABS_{560}) - 6.11 \quad (4)$$

$$C_S = 3.12(ABS_{560}) - 4.52 \quad (5)$$

Calculation of total biomass

Biofilm quantification was achieved by physically removing the biofilm from the internal surface of the bioreactor. All feed to the bioreactor was ceased while simultaneously increasing the shear velocity in the bioreactor to 3.65 $m.s^{-1}$ for 30 minutes, to ensure total removal of the biofilm. During this period, the biofilm was "scrubbed" from the internal surface of the reactor section and thoroughly mixed due to the significant shear and turbulence in the reactor. In order to keep the reactor ready for subsequent experiments, without the need for a complete restart, the reactor was not completely drained. Rather, after 30 min the feed rate was increased to the maximum flow of 8.6 $mL.min^{-1}$ while the recycle velocity was kept at 3.65 $m.s^{-1}$ and a sample of approximately 20 mL was taken from the reactor. The exact sample size (V_S) was determined by weight.

Assuming negligible growth of cells during the washout procedure, the initial biomass concentration (C_o) in the reactor was modelled as a two-tank system with flow of liquid through the first constant-volume tank (fermenter V_R) and accumulation of liquid in the second tank (sample V_S). C_o was calculated using the theoretically derived equation (6).

$$C_o = \frac{C_S}{\frac{V_R}{V_S}\left(1 - e^{-\frac{V_S}{V_R}}\right)} \quad (6)$$

RESULTS AND DISCUSSION

The dataset represents 21 steady state conditions. Four velocity or shear conditions were investigated while the dilution rates (D) were varied between values of 0.1 h^{-1} to 0.7 h^{-1}. Each shear condition comprised four to six separate dilution rates. C_{HLac},

C_{Acn}, C_x and total biomass concentration (C_{xt}), i.e. sum of attached and suspended biomass (x_t), were quantified at each of the 21 steady states. All D values only resulted in partial Glc conversion, with the C_{Glc} in the outlet always exceeding 5 g/ L.

Biofilm characteristics

The C_{xt} and C_x biomass measurements are given as a function of D in Figure 4. The chemostat run, consisting of only x, exhibits the expected behaviour with a decline in C_x as D increases. Despite prolonged operation of the biofilm runs no clear trend is observable with regards to the C_{xt} measurements. The C_x of the biofilm runs was in close proximity to that of the chemostat run, while C_{xt} were generally higher at lower shear velocities. Repeat runs at similar dilution rates (u=0.37, D=0.2 and D=0.6) did not result in repeatable C_{xt}, although steady state was established. This is in agreement with the work of Peyton & Characklis [32] and Peyton [33], who observed significant variation in biofilm thickness, roughness and density for constant substrate loadings (analogous to dilution rate) and shear conditions.

In Figure 5 the C_x to C_{xt} are shown, with the fitted average ratio of suspended-to-total biomass (C_x/C_{xt}) for each shear condition given as the slope and expressed as a yield ($Y_{xt,x}$). In Figure 5 the independent variable D is not directly observable due to the random variations observed in the measured concentrations (Figure 4). The $Y_{xt,x}$ remains strikingly constant at a specific shear, despite the fluctuations in the C_x and C_{xt} (Figure 4). Furthermore, a clear decrease in the $Y_{xt,x}$ is observed as the u decreases. The lowest fitted $Y_{xt,x}$ of 0.61 at a u of 0.19 m s^{-1} indicates that the C_x is greater than the attached biomass concentration, even at the lowest shear condition. This coincided with the visual observation of the biofilm where the biofilm appeared thin and non-evenly dispersed over the internal tube area

The constant $Y_{xt,x}$ at a given shear condition was attributed to a constant balance between the biofilm growth and detachment. The balance is clearly related to u where higher shear increase the rate of detachment [34–36]. Given the rapid detachment rate of biofilm and the relatively low ratio of suspended to total biomass (between 0.61 $g.g^{-1}$ and 0.79 $g.g^{-1}$), it was assumed that the composition of the x and immobilised biomass for each respective shear condition was the same and remained constant irrespective of D.

Yield and rate analysis

The observed product and biomass yields are given in Figures 6-8. Glc consumption is used as basis for all yield determinations and plotted on the horizontal axis of Figure 6-8. The linear fit on these graphs give the observed yield coefficients with the regression analysis indicated on the graphs. The independent variable D is not directly observable in this figures but can be inferred from the fact that high D will result in low Glc consumption.

A significant change in the HLac and Acn yield ($Y_{Glc,HLac}$ and $Y_{Glc,Acn}$) is observed with a change in shear, while the biomass yield based on the suspended biomass exiting the fermenter ($Y_{Glc,x}$) remains more or less constant with shear variation. The Acn yield increases more than fourfold from the lowest shear biofilm run ($Y_{Glc,Acn}$=0.017 $g.g^{-1}$) to the chemostat run ($Y_{Glc,Acn}$=0.074 $g.g^{-1}$). The HLac yield decreased by 20% from the highest value obtained in the lowest shear biofilm run ($Y_{Glc,Hlac}$=0.9 $g.g^{-1}$) to that of the chemostat run ($Y_{Glc,Hlac}$=0.75 $g.g^{-1}$).

From Figure 6 and Figure 7, it is clear from the regression statistics that the yields of the metabolic products remained remarkably constant for each respective u. Since both growth and maintenance [20,37] are expected to contribute to metabolite production, the measured or observed yield can be described by the following equation:

$$Y_{Glc,P}^{obs} = \frac{r_P}{r_{Glc}} = \frac{Y_{x,P}^{true}\mu + m_P}{Y_{x,Glc}^{true}\mu + m_{Glc}} \approx \frac{Y_{x,P}^{true}}{Y_{x,Glc}^{true}} \quad (7)$$

For HLac production the maintenance constants m_{Pi} and m_{Glc} are identical since no loss of mass occurs in the formation of HLac. The growth rate (μ) will vary according to different amounts of HLac in the broth causing varying degrees of inhibition. Since the observed yield ($Y_{Glc,P}^{obs}$) remains constant while the HLac titre (and μ) is changing, it is evident that m_P (and m_{Glc}) is negligibly small in order for μ to cancel out of the equation. Accordingly, maintenance or non-growth effects can be ignored within the dilution rate range of the study.

Figure 9 shows the biomass-based rates of Glc consumption (r_{Glc}) and HLac production (r_{HLac}). Note that the C_{xt} was used for the calculation of the specific rates. At high D a distinct decrease in biomass productivity is observed at lower u. At high

D, where the biomass productivity differences are observed, HLac titres are low and product inhibition is at a minimum. The cellular part of the biomass (x_c) at these conditions is expected to have similar metabolite production characteristics irrespective of the shear on the biofilm (Biofilm characteristics section). Accordingly the decrease in biomass productivity can only be attributed to metabolically inactive biomass like EPS. The rate results therefore suggest that the EPS fraction of the biomass increases with a decrease in shear.

NADH balance for elucidating flux variation

The major variation of metabolite yields with shear requires further exploration. A clue to understanding the observation lies in the redox difference between HLac and Acn. The overall metabolic pathway from glucose to Acn is associated with the generation of NADH and it is well accepted that Acn production is linked to the regulation of NAD^+/NADH in a microbial system [38]. In comparison to Acn production from glucose HLac production is redox neutral. Since the net NADH production in the cell should be zero, it is clear that NADH consumption is related to the shear condition in the fermenter where less NADH is consumed at low shear conditions. NADH consumption can only proceed via the anabolism or via the direct oxidation of NADH since all the catabolites are quantified. The direct oxidation option is unlikely since the system was proven to be completely anaerobic (*Product analysis* section). It is well established that biomass growth on inorganic nitrogen is associated with the formation of NADH, while growth on complex and undefined organic nitrogen is considered to be redox neutral [20]. For interpretation purposes it was decided to associate the apparent NADH consumption with the formation of cellular biomass.

If the hypothesis holds that redox is consumed in the formation of biomass, x formation under lower u would necessarily consume less redox (NADH). This is because the $Y_{Glc,Acn}$ drastically decreased at lower shear conditions while the $Y_{Glc,x}$ remained unchanged. When considering the rate data in Figure 9 one can attribute the rate decrease to a change in the biomass composition, where more inactive EPS are present at lower shear conditions, thus lowering the productivity of the x_t. This observation can be used to elucidate the redox consumption changes where it is proposed that EPS formation is different to cellular biomass formation in terms of

NADH consumption/production. *L. rhamnosus* is known to produce EPS with the following repeating unit: {3Rha-3Glc-3[Gal4,6(R)Py-2]Rha-3Rha-3Rha-2Glc-}$_n$ [23]. This can be used to calculate the overall NADH consumption/production when forming EPS from Glc. The underlying assumption is that the EPS fraction in the biomass is independent of dilution rate due to the fact that the substrate is always present in excess. Variations in EPS content has been reported at substrate inhibition conditions [39].

The complete metabolism can be represented by two catabolic reactions (HLac and Acn) and two anabolic reactions (x_c and EPS). The carbon flux of these reactions was converted to a carbon mole basis (C-mol.L^{-1}) and the degree of reduction (DOR) of the components was determined by using H_2O, CO_2 and NH_3 as the defined neutral compounds. The metabolism can be written as equations (8) to (11) indicating four separate fluxes (v_1 – v_4). The cellular biomass (x_c) flux (v_3) is separated from EPS flux (v_4).

$$v_1: CH_2O\ (Glc) \rightarrow CH_2O\ (HLac) \tag{8}$$

$$v_2: CH_2O\ (Glc) \rightarrow \frac{2}{3}CH_2O_{0.5}\ (Acn) + \frac{1}{3}CO_2 + \frac{1}{3}NADH \tag{9}$$

$$v_3: CH_2O\ (Glc) + 0.59YE \rightarrow 1.59x_c + Y_3NADH \tag{10}$$

$$v_4: CH_2O\ (Glc) \rightarrow EPS + Y_4NADH \tag{11}$$

The chemostat run was used as the baseline scenario with the assumption that zero EPS formed in this run ($v_4 = 0$, $x_c = x$). Given the measured values of HLac and Acn produced, and Glc consumed, the fluxes v_1 and v_2 were determine to be 0.9 (C-mol Glc)/(total C-mol Glc consumed). Y_3 was determined to be -0.42, using the known fluxes and an NADH balance. CO_2 formation during biomass synthesis was not considered ($\alpha = 0$). Note that the Glc flux in v_3, expressed as a fraction of the total Glc consumed, was calculated by using only the C_{HLac}, C_{Acn} and C_{Glc} measurements. The x_c and YE yield coefficients were determined from the $Y_{Glc,x}$, assuming a biomass composition of $CH_{1.8}O_{0.5}N_{0.2}$ [20].

When considering the biofilm runs, the combined ($v_3 + v_4$) flux was shown to vary between 0.06 and 0.09 (C-mol Glc)/(total C-mol Glc consumed). This value is slightly lower than expected and is most likely due to small inaccuracies in the Acn and

HLac yield fits. The yield coefficient (Y_3) of equation (10) were determined for the chemostat run and directly applied in the biofilm runs. Using the known EPS composition ($CH_{1.6}O_{0.89}$) from the repeating unit given above, a redox balance was used to calculate Y_4 (0.09 moles NADH ***formed*** per C-mol EPS).
Therefore the overall NADH balance dictated the increased yield of EPS (v_4) production and the decreased yield of cellular biomass production (v_3) with the decrease in Acn production (v_2). Using the proposed anabolic stoichiometry, the EPS fraction of the biomass was estimated with equation (12), from values for v_3 and v_4 from Table 1. The results are reported in Table 1.

$$\text{EPS fraction} = \frac{v_4}{v_4 + 1.59v_3} \tag{12}$$

CONCLUSIONS

This study clearly illustrated that shear can affect the metabolite yields of *L. rhamnosus* biofilms. Increasing shear resulted in decreased Acn formation and increased HLac formation while biomass yields remained constant. Rate data indicated a lower specific biomass productivity with shear decrease, suggesting a composition change in biomass where more inactive EPS forms part of the biomass at low shear velocities.

Redox analysis of the catabolic reactions revealed that the anabolic reactions are associated with the net consumption of NADH, despite the fact that EPS production was calculated to be an NADH producer. The decrease of Acn formation with decreasing shear clearly indicated that the extent of anabolic NADH consumption was related to shear. The relationship was explained by varying the EPS content of the biomass as a function of shear velocity, which coincides with the rate findings. A simplified model was presented to estimate the distribution of EPS and cellular biomass as the shear varied.

This study highlights the potential of biofilm cells for altering yields in fermentations. With proper understanding of biofilms, metabolic flux can be manipulated in order to enhance the yield of the desired metabolite. With improved productivity due to high cell densities and the possibility of improved yields, pure culture biofilm reactors are likely to receive more attention in years to come.

Glossary

ABS_{560}	Absorption of light with wavelength 560 nm	(-)
Acn	Acetoin	
ATP	Adenosine triphosphate	
$C_{HLac}(t)$	Concentration of HLac at time t	($g.L^{-1}$)
$C_{HLac,steady}$	Predicted concentration of HLac at steady state	($g.L^{-1}$)
C_o	C_{xt} in the reactor prior to washout	($g.L^{-1}$)
C_S	C_{xt} in the sample vial after washout	($g.L^{-1}$)
C_i	Concentration of component i in the reactor	($g.L^{-1}$)
D	Overall dilution rate through the reactor	(h^{-1})
Diac	diacetyl	
DOR	Degree of reduction	
EPS	Extracellular polymeric substances	
Glc	Glucose	
HLac	Lactic acid	
HPyr	Pyruvic Acid	
m_{Glc}	Specific Glc consumption rate during maintenance	($g.g^{-1}.h^{-1}$)

m_P	Specific Product P production rate during maintenance	$(g.g^{-1}.h^{-1})$
MRS	de Man, Rogosa and Sharpe	
NAD^+/NADH	Nicotinamide adenine dinucleotide	
$q_{HLac}(t)$	Volumetric production rate of HLac at time t	$(g.L^{-1}h^{-1})$
$Q_{NaOH}(t)$	Volumetric flow rate of NaOH at time t	$(L.h^{-1})$
r_{Glc}	Specific consumption rate of Glc in the system	$(g.g^{-1}.h^{-1})$
r_P	Specific production rate of product P in the system	$(g.g^{-1}.h^{-1})$
Δt	Sampling period of data logging system	(h)
t_f	Time at which the experimental run was terminated	(h)
u	Superficial recycle velocity or shear velocity	$(m.s^{-1})$
v_1	Metabolic flux of Glc to HLac	$C\text{-}mol.h^{-1}$
v_2	Metabolic flux of Glc to Acn, CO_2 and NADH	$C\text{-}mol.h^{-1}$
v_3	Metabolic flux of Glc and YE to x_c and NADH	$C\text{-}mol.h^{-1}$
v_4	Metabolic flux of Glc to EPS and NADH	$C\text{-}mol.h^{-1}$
V_R	Volume of reactor	(L)
V_S	Volume captured in the sample vial during the washout procedure	(L)

x	Suspended biomass	
x_c	Cellular biomass	
x_t	Total biomass	
Y_3	NADH requirements for biomass production	(mol.C-mol^{-1})
Y_4	NADH production for EPS production	(mol.C-mol^{-1})
$Y_{x,Glc}^{true}$	True yield of Glc to x	(g.g^{-1})
$Y_{Glc,x}^{obs}$	Observed yield of x to Glc consumed	(g.g^{-1})
$Y_{x,Glc}^{true}$	True yield of Glc to x consumed	(g.g^{-1})
$Y_{Glc,P}$	Yield of metabolite P to Glc consumed	(g.g^{-1})
$Y_{xt,x}$	Yield of x to x_t in the system	(g.g^{-1})
YE	Yeast extract	
α	Yield of CO2 production to biomass	(g.g^{-1})
μ	Specific growth rate of biomass	(g.g^{-1}.h^{-1})

References

[1] Dagher SF, Ragout AL, Siñeriz F, Bruno-Bárcena JM. Cell immobilization for production of lactic acid biofilms do it naturally. Adv Appl Microbiol 2010;71:113–48.

[2] Karel SF, Libicki SB, Robertson CR. The immobilization of whole cells: Engineering principles. Chem Eng Sci 1985;40:1321–54.

[3] Nicolella C, van Loosdrecht MC, Heijnen JJ. Wastewater treatment with particulate biofilm reactors. J Biotechnol 2000;80:1–33.

[4] Qureshi N, Annous BA, Ezeji TC, Karcher P, Maddox IS. Biofilm reactors for industrial bioconversion processes: employing potential of enhanced reaction rates. Microb Cell Fact 2005;4:24.

[5] Xu J, Guo B-H. Poly(butylene succinate) and its copolymers: research, development and industrialization. Biotechnol J 2010;5:1149–63.

[6] Rosche B, Li XZ, Hauer B, Schmid A, Buehler K. Microbial biofilms: a concept for industrial catalysis? Trends Biotechnol 2009;27:636–43.

[7] Zhang W, Sileika TS, Chen C, Liu Y, Lee J, Packman AI. A novel planar flow cell for studies of biofilm heterogeneity and flow-biofilm interactions. Biotechnol Bioeng 2011;108:2571–82.

[8] Agathos SN, Hellin E, Ali-Khodja H, Deseveaux S, Vandermesse F, Naveau H. Gas-phase methyl ethyl ketone biodegradation in a tubular biofilm reactor: microbiological and bioprocess aspects. Biodegradation 1997;8:251–64.

[9] Maharaj K, Bradfield MFA, Nicol W. Succinic acid-producing biofilms of Actinobacillus succinogenes: reproducibility, stability and productivity. Appl Microbiol Biotechnol 2014.

[10] Beyenal H, Lewandowski Z. Internal and external mass transfer in biofilms grown at various flow velocities. Biotechnol Prog 2002;18:55–61.

[11] Stoodley P, Yang S, Lappin-Scott H, Lewandowski Z. Relationship between mass transfer coefficient and liquid flow velocity in heterogenous biofilms using microelectrodes and confocal microscopy. Biotechnol Bioeng 1997;56:681–8.

[12] Fernando S, Adhikari S, Chandrapal C, Murali N. Biorefineries: Current Status, Challenges, and Future Direction. Energy & Fuels 2006;20:1727–37.

[13] Gavrilescu M, Chisti Y. Biotechnology-a sustainable alternative for chemical industry. Biotechnol Adv 2005;23:471–99.

[14] Hoskisson P a, Hobbs G. Continuous culture--making a comeback? Microbiology 2005;151:3153–9.

[15] Gross R, Hauer B, Otto K, Schmid A. Microbial biofilms: new catalysts for maximizing productivity of long-term biotransformations. Biotechnol Bioeng 2007;98:1123–34.

[16] Liu Y, Tay J-H. The essential role of hydrodynamic shear force in the formation of biofilm and granular sludge. Water Res 2002;36:1653–65.

[17] Mattos MJT, Boer JP, Zoutberg GR, Neijssel OM. Metabolic shift analysis at high cell densities. FEMS Microbiol Rev 1994;14:21–8.

[18] Bradfield MFA, Nicol W. Continuous succinic acid production by Actinobacillus succinogenes in a biofilm reactor: Steady-state metabolic flux variation. Biochem Eng J 2014;85:1–7.

[19] Nielsen J. It Is All about Metabolic Fluxes. J Bacteriol 2003;185:7031–5.

[20] Villadsen J, Nielsen J, Lidén G. Bioreaction Engineering Principles. 3rd Editio. Boston, MA: Springer US; 2011.

[21] Laspidou CS, Rittmann BE. A unified theory for extracellular polymeric substances, soluble microbial products, and active and inert biomass. Water Res 2002;36:2711–20.

[22] Bergmaier D, Champagne CP, Lacroix C. Growth and exopolysaccharide production during free and immobilized cell chemostat culture of Lactobacillus rhamnosus RW-9595M. J Appl Microbiol 2005;98:272–84.

[23] Van Calsteren MR, Pau-Roblot C, Bégin A, Roy D. Structure determination of the exopolysaccharide produced by Lactobacillus rhamnosus strains RW-9595M and R. Biochem J 2002;363:7.

[24] Kim J, KIM Y, Han K, OH S, Whang K, Kim J, et al. Function of cell-bound and released exopolysaccharides produced by Lactobacillus rhamnosus ATCC 9595. J Microbiol Biotechnol 2006;16:939–45.

[25] Dupont I, Roy D, Lapointe G. Comparison of exopolysaccharide production by strains of Lactobacillus rhamnosus and Lactobacillus paracasei grown in chemically defined medium and milk. J Ind Microbiol Biotechnol 2000;24:251–5.

[26] Bakke R, Kommedal R, Kalvenes S. Quantification of biofilm accumulation by an optical approach. J Microbiol Methods 2001;44:13–26.

[27] Poolman MG, Venkatesh K V, Pidcock MK, Fell D a. A method for the determination of flux in elementary modes, and its application to Lactobacillus rhamnosus. Biotechnol Bioeng 2004;88:601–12.

[28] Gayen K, Gupta M, Venkatesh K V. Elementary mode analysis to study the preculturing effect on the metabolic state of Lactobacillus rhamnosus during growth on mixed substrates. In Silico Biol 2007;7:123–39.

[29] Jyoti BDD, Suresh AKK, Venkatesh KV V. Effect of preculturing conditions on growth of Lactobacillus rhamnosus on medium containing glucose and citrate. Microbiol Res 2004;159:35–42.

[30] Park SH, Xing R, Whitman WB. Nonenzymatic acetolactate oxidation to diacetyl by flavin, nicotinamide and quinone coenzymes. Biochim Biophys Acta - Gen Subj 1995;1245:366–70.

[31] Oliveira AP, Nielsen J, Förster J. Modeling Lactococcus lactis using a genome-scale flux model. BMC Microbiol 2005;5:39.

[32] Peyton BM, Characklis WG. A statistical analysis of the effect of substrate utilization and shear stress on the kinetics of biofilm detachment. Biotechnol Bioeng 1993;41:728–35.

[33] Peyton B. Effects of shear stress and substrate loading rate on Pseudomonas aeruginosa biofilm thickness and density. Water Res 1996;30:29–36.

[34] Van Loosdrecht MCM, Eikelboom D, Gjatelma A, Mulder A, Tijhuis L, Heijnen JJ. Biofilm structures. Water Sci Technol 1995;32:35–43.

[35] Van Loosdrecht MCM, Picioreanu C, Heijnen JJ. A more unifying hypothesis for biofilm structures. FEMS Microbiol Ecol 2006;24:181–3.

[36] Van Loosdrecht MCM, Heijnen JJ, Eberl H, Kreft J, Picioreanu C. Mathematical modelling of biofilm structures. Antonie Van Leeuwenhoek 2002;81:245–56.

[37] Luedeking R, Piret EL. A kinetic study of the lactic acid fermentation. Batch process at controlled pH. Reprinted from Journal of Biochemical and Microbiological Technology Engineering Vol. I, No. 4. Pages 393-412 (1959). Biotechnol Bioeng 2000;67:636–44.

[38] Xiao Z, Xu P. Acetoin metabolism in bacteria. Crit Rev Microbiol 2007;33:127–40.

[39] Looijesteijn PJ, van Casteren WH, Tuinier R, Doeswijk-Voragen CH, Hugenholtz J. Influence of different substrate limitations on the yield, composition and molecular mass of exopolysaccharides produced by Lactococcus lactis subsp. cremoris in continuous cultures. J Appl Microbiol 2000;89:116–22.

Table captions

Table 1: Biomass flux distribution (v_3 and v_4) as well as the EPS fractions calculated for the respective shear velocities

Figure captions

Figure 1: Fermenter setup (the reactor section is shown in bold)

Figure 2: Metabolic flux diagram for *L. rhamnosus* (adapted from literature [27-29])

Figure 3: Predicted transient and steady state lactic acid concentrations as calculated during an experimental run at $D \approx 0.32\ h^{-1}$ and a recycle velocity of $0.55\ m.s^{-1}$

Figure 4: Suspended and total biomass concentrations ($g.L^{-1}$). The suspended biomass concentrations were inferred from equation (4) the total biomass concentrations from equation (5) and adjusted for dilution by equation (6).

Figure 5: Suspended biomass ($g.L^{-1}$) vs. total biomass ($g.L^{-1}$) to determine $Y_{xt,x}$. The suspended biomass concentrations were inferred from equation (4) the total biomass concentrations from equation (5) and adjusted for dilution by equation (6).

Figure 6: HLac production ($g.L^{-1}$) vs. Glc consumption ($g.L^{-1}$) to determine $Y_{Glc,HLac}$ for the 4 individual shear velocities. The individual data points were for the respective dilution rates (D) with the lowest D corresponding to the highest Glc consumption.

Figure 7: Acn production ($g.L^{-1}$) vs. Glc consumption ($g.L^{-1}$) to determine $Y_{Glc,Acn}$ for the 4 individual shear velocities. The individual data points were for the respective dilution rates (D) with the lowest D corresponding to the highest Glc consumption.

Figure 8: Suspended biomass ($g.L^{-1}$) vs. Glc consumption ($g.L^{-1}$) to determine $Y_{Glc,x}$ for the 4 individual shear velocities. The individual data points were for the respective dilution rates (D) with the lowest D corresponding to the highest Glc consumption.

Figure 9: a) Specific Glc consumption rate (r_{Glc}); b) Specific HLac production rate (r_{HLac}) against dilution rate

Table 1: Biomass flux and EPS fractions

Shear Velocity ($m.s^{-1}$)	v_3 (C-mol.C-mol^{-1})	v_4 (C-mol.C-mol^{-1})	EPS fraction
3.65 (chemostat)	0.10	0.00	0.00
0.55	0.06	0.01	0.09
0.37	0.04	0.05	0.43
0.19	0.01	0.05	0.70

Figure 1: Fermenter setup

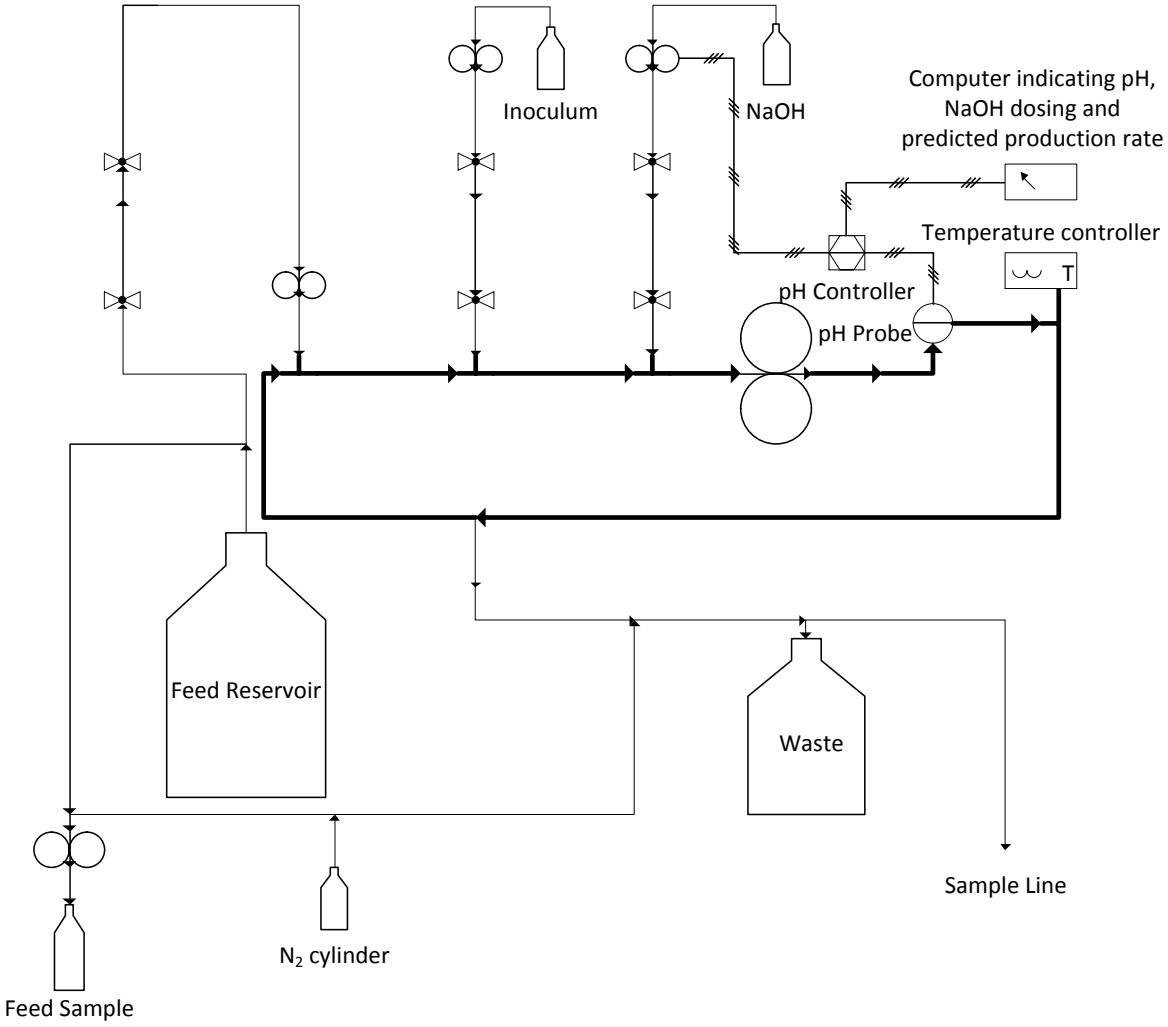

Figure 2: Metabolic flux diagram for L. rhamnosus

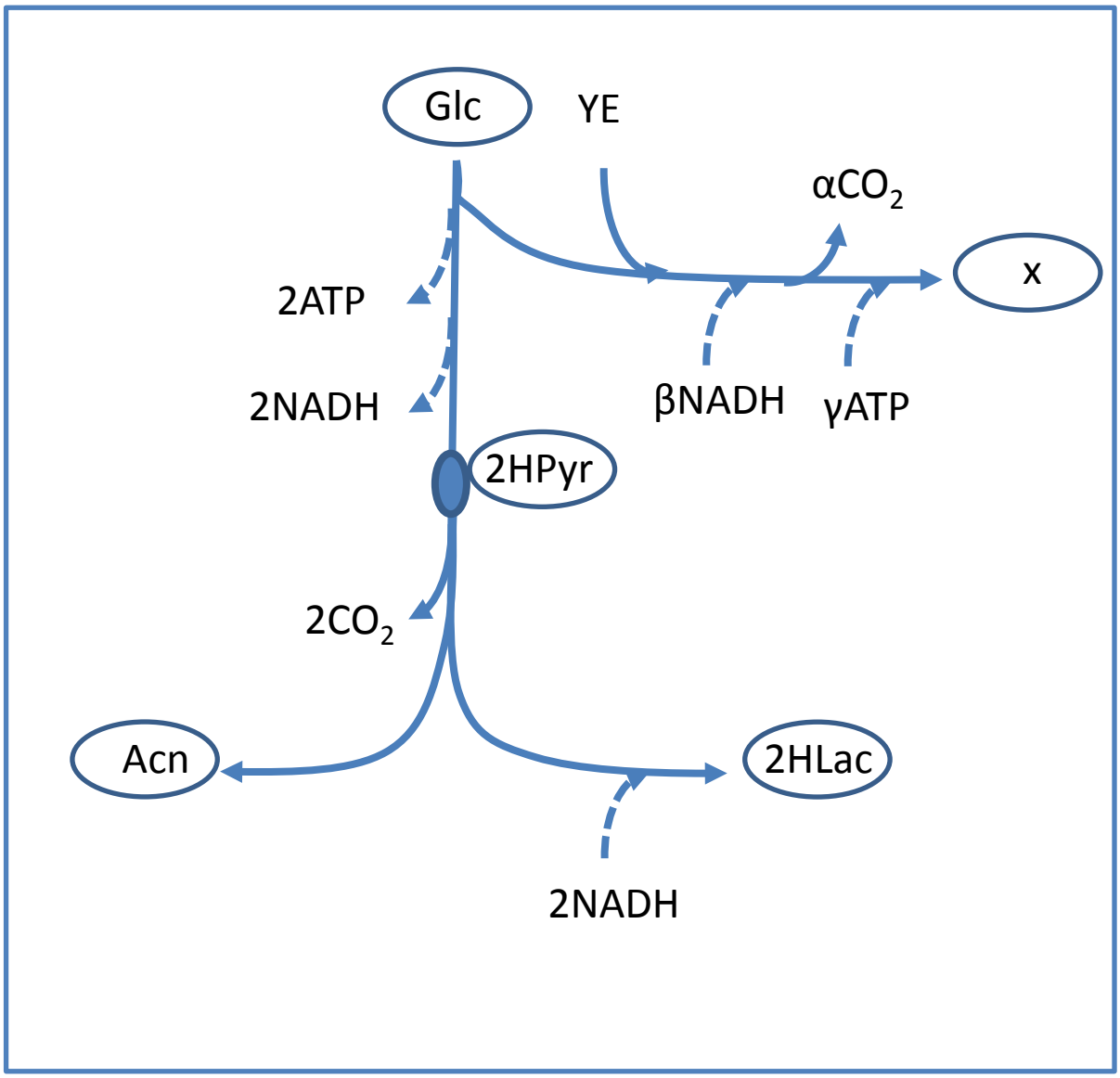

Figure 3: Predicted transient and steady state lactic acid conce

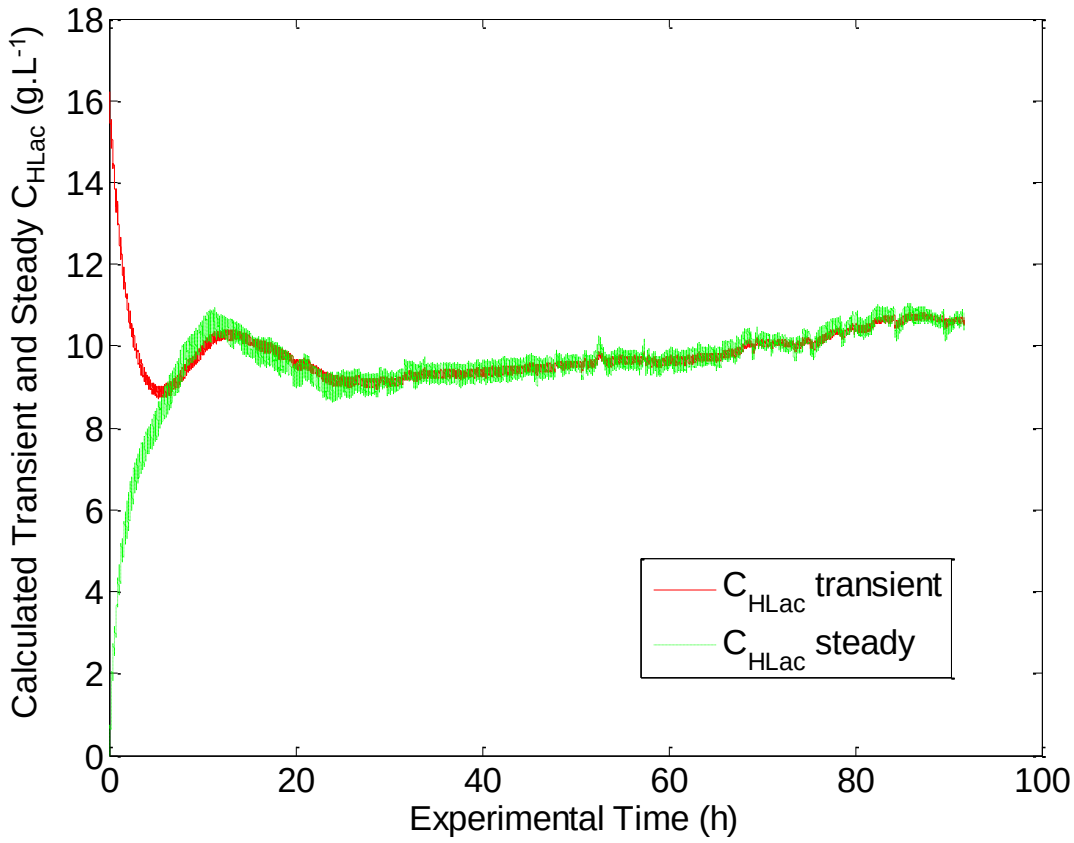

Figure 4: Suspended and total biomass concentrations (g/L).

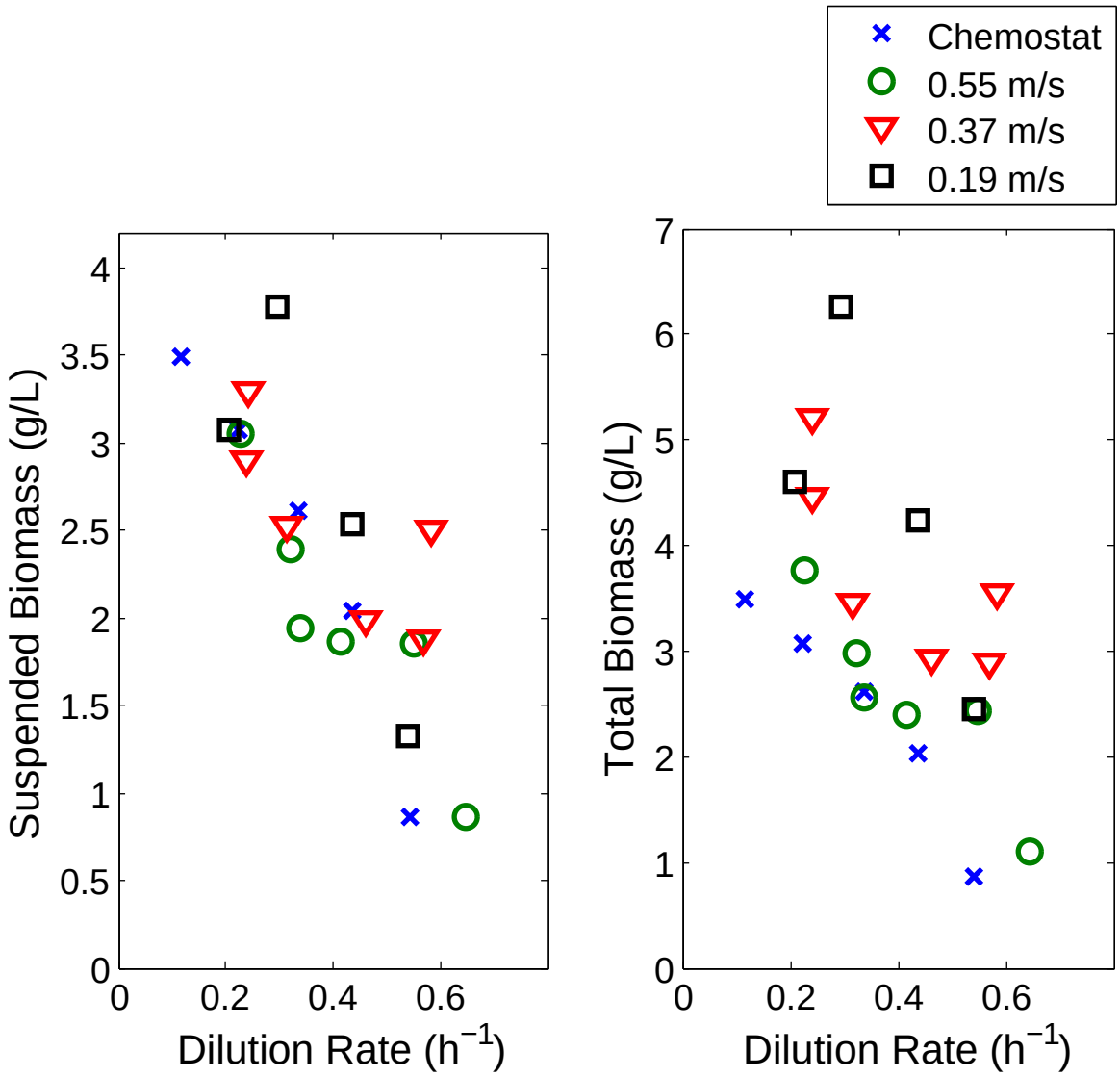

Figure 5: Suspended biomass (g/L) vs. total biomass (g/L)

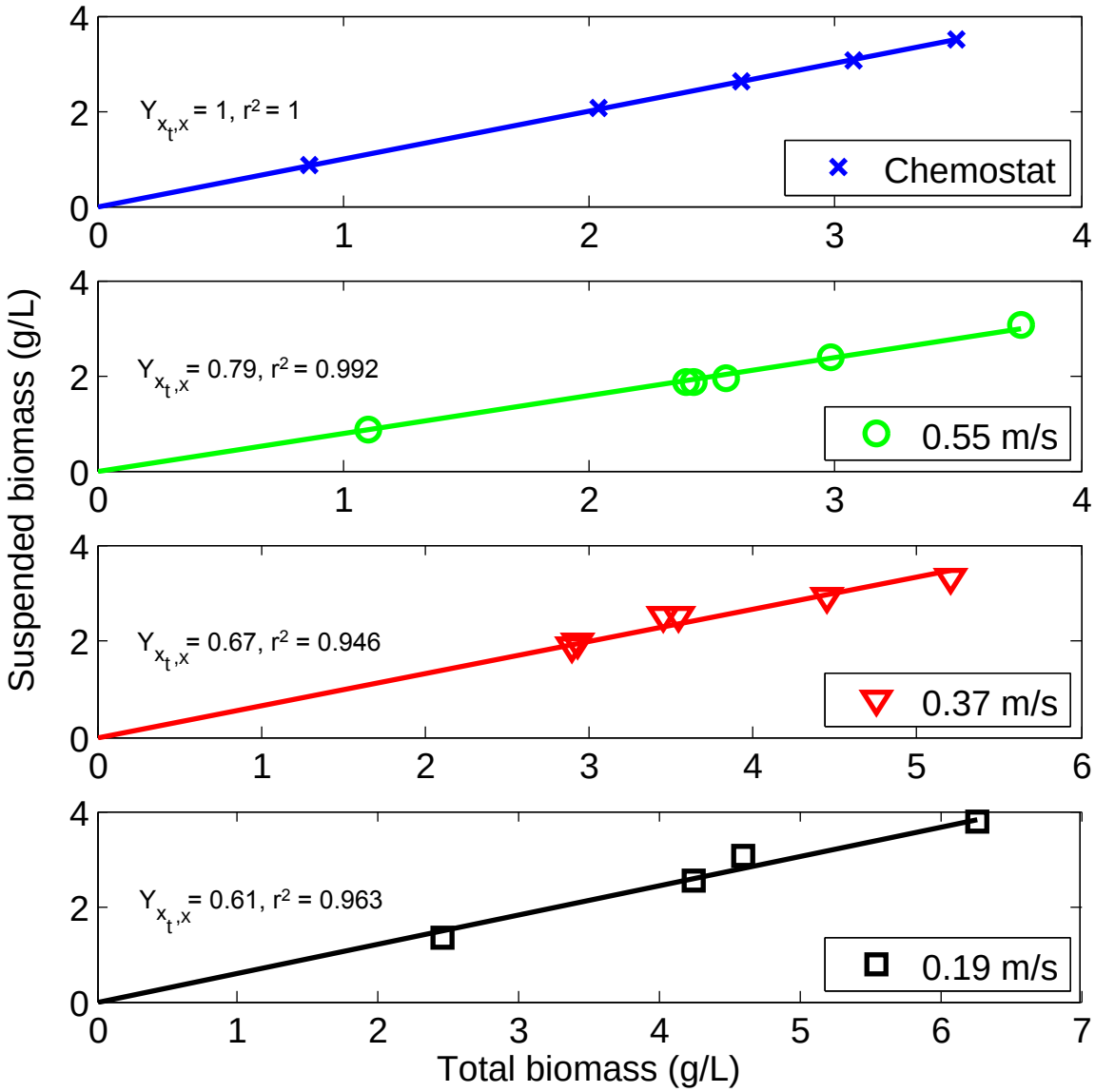

Figure 6: HLac production (g/L) vs. Glc consumption (g/L)

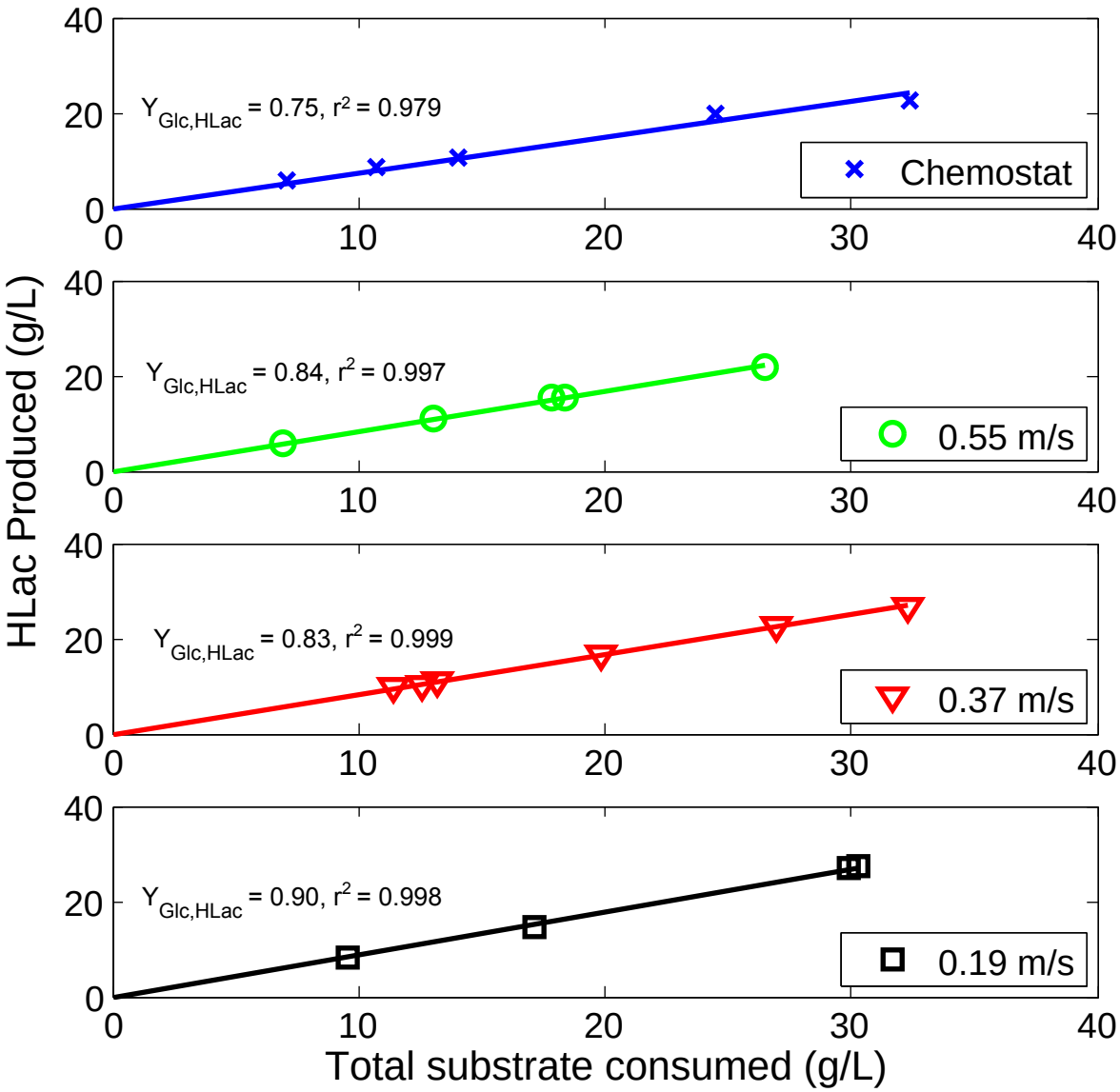

Figure 7: Acn production (g/L) vs. Glc consumption (g/L)

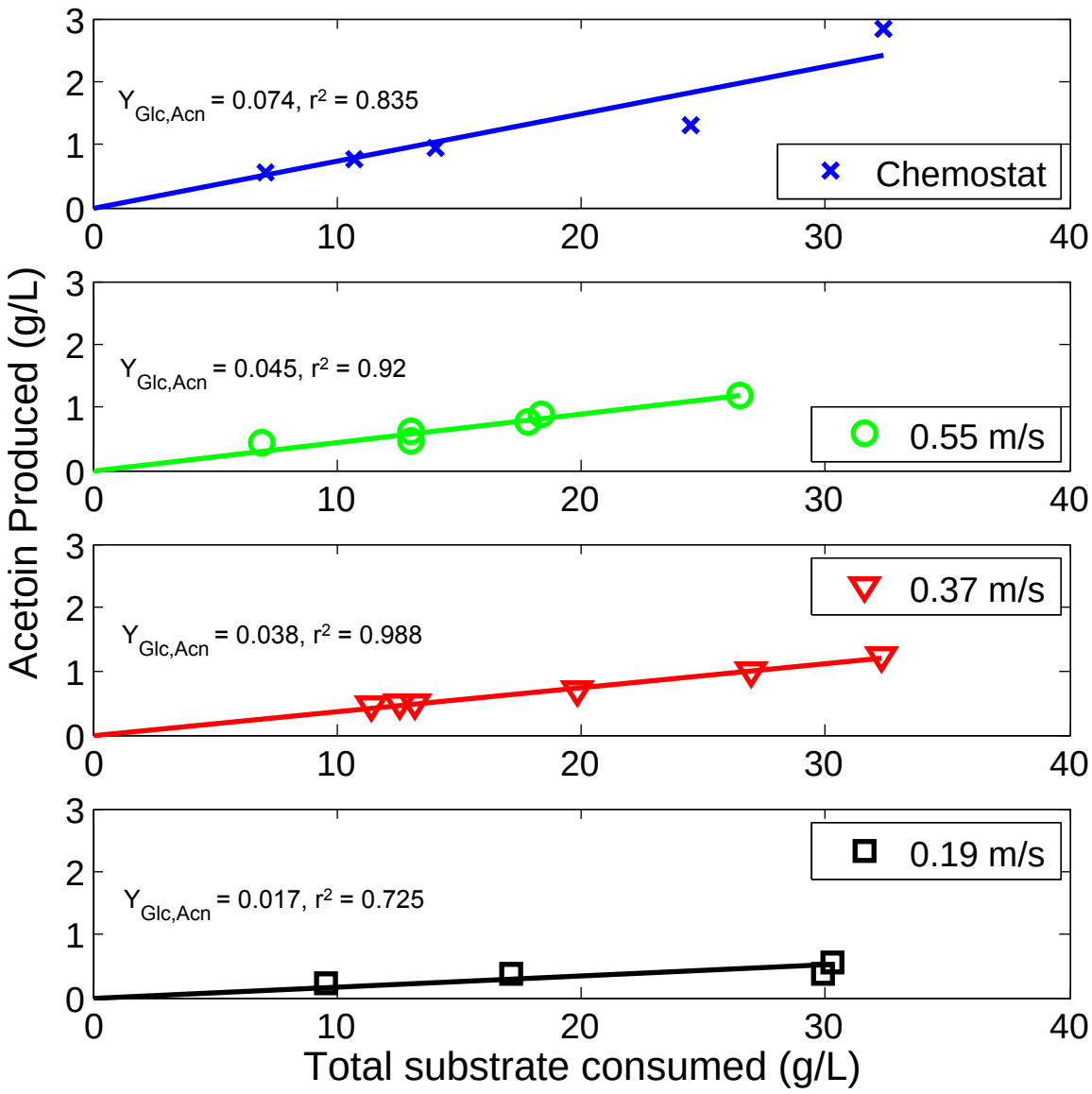

Figure 8: Suspended biomass (g/L) vs. Glc consumption (g/L)

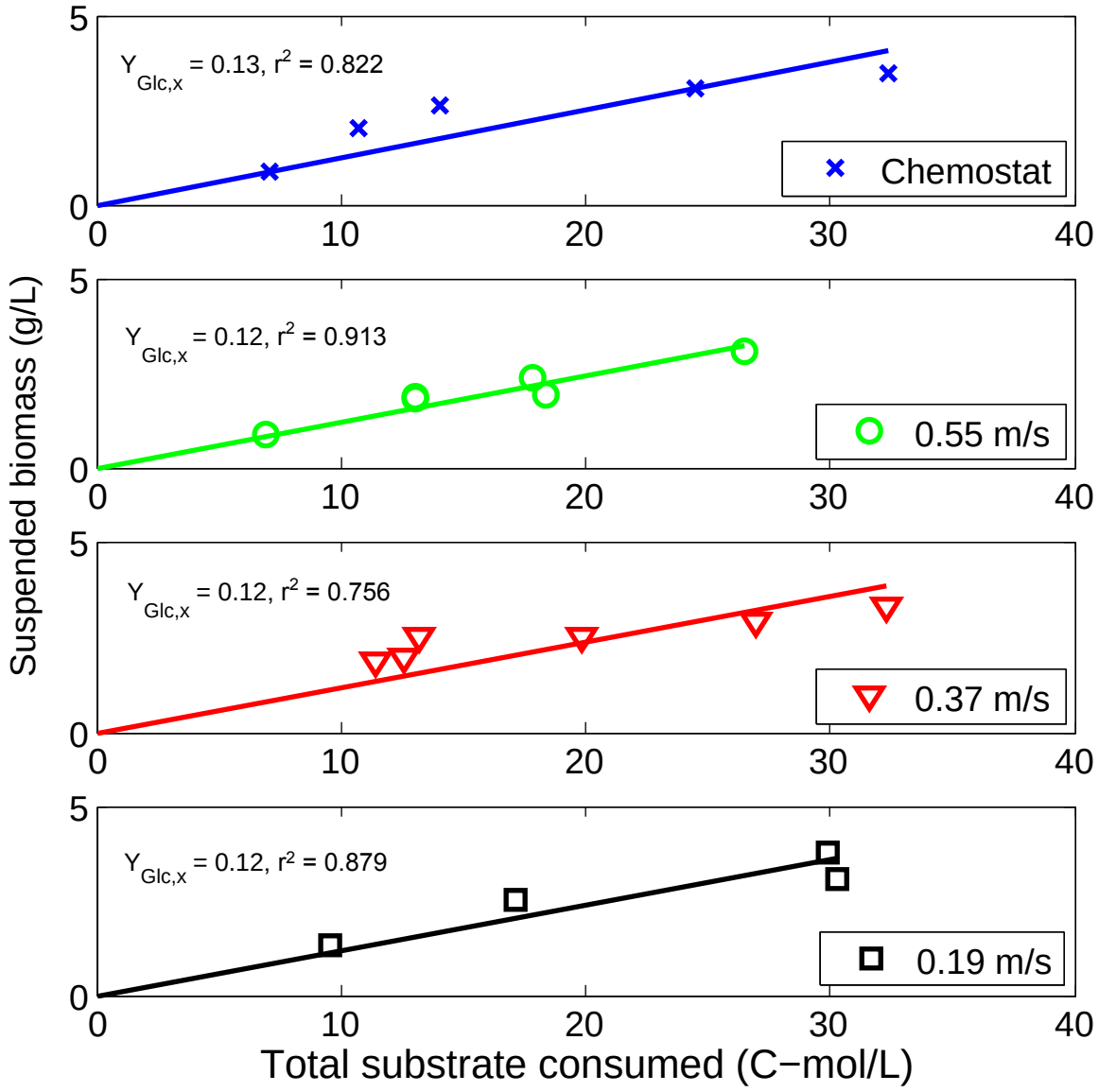

Figure 9: a) rGlc vs D; b) rHLac vs D